

Date of publication xxxx 00, 0000, date of current version xxxx 00, 0000.

Digital Object Identifier 10.1109/ACCESS.2023.0322000

Quantum Sensing of Fast Time-Varying Magnetic Field With Daubechies Wavelets

CHOU-WEI KIANG¹, JIAN-JIUN DING^{1 2}, (Senior Member, IEEE), and JEAN-FU KIANG^{1 2}, (Life Senior, IEEE)

¹Department of Electrical Engineering, National Taiwan University, Taipei, Taiwan 10617

²Graduate Institute of Communication Engineering, National Taiwan University, Taipei, Taiwan 10617

Corresponding author: Jean-Fu Kiang (email: jfkiang@ntu.edu.tw.).

ABSTRACT

A quantum sensing protocol is proposed to apply continuous-wave microwave sequences modulated by Daubechies wavelets to control quantum sensors. The Daubechies wavelet coefficients thus extracted are used to reconstruct a fast time-varying magnetic field with higher smoothness, mitigating square-shaped artifacts as Haar wavelets or Walsh functions are used for modulation. The relations between the qubit readout, the accumulated phase of the quantum state, and the wavelet coefficients are derived based on an intuitive model represented on the Bloch sphere. The efficacy and accuracy of the proposed waveform reconstruction method under various conditions are evaluated by simulations.

INDEX TERMS quantum sensing, quantum control, wavelet analysis, time-varying signal, waveform reconstruction, magnetometry

I. INTRODUCTION

High-sensitivity quantum sensors have versatile applications in sensing and imaging electric fields [1], [2], magnetic fields [3], [4], temperature [5], pressure [6], and strain [7]. They have been widely used for sensing dc magnetic fields [3] and ac ones [8] over the past decade, as well as noise [9] and time-varying signal [10], [11], [12].

Quantum sensing of fast time-varying waveforms is promising in navigation, environmental monitoring [13], measuring geomagnetic field fluctuations of seismo-ionospheric interaction [14], non-invasive detection of biological signals like the magnetic field induced by neural action potential [15] and nerve impulses [16], studying condensed matter physics like photo-current [17] and dynamics of spin-orbit torque-driven magnetization [18].

A time-varying magnetic field can be pieced together via consecutive differential detection of short signal segments [10], but is limited to signals that can be repeated within the coherence time of a quantum sensor. In contrast, coherent control-based methods are free of such constraints in reconstructing a time-varying field. For example, qubits can be manipulated with microwave (MW) control sequences, which mimic orthogonal basis functions, such as the Haar wavelet [11] or Walsh functions [12], to extract the weighting coefficients. An inverse transform is then applied to reconstruct the time-varying signal from these coefficients.

However, the piece-wise constant waveform of Haar and Walsh functions results in step-like artifacts in the reconstructed signal. More complex orthogonal basis functions can be used to modulate the MW control sequences exerted on qubits [19]. In [9], a control protocol based on the discrete prolate spheroidal sequences (DPSS) was proposed to mitigate spectral leakage in noise spectroscopy.

Daubechies wavelets, with higher vanishing moments, can be adopted for quantum sensing to achieve smoother reconstruction of arbitrary time-varying waveforms. Let us label a function with continuous α th derivative as a C^α function. Functions with higher α are smoother, and α of a mother wavelet function is proportional to the number of its vanishing moments [20]. Thus, some specific functions can be well approximated with only a few nonzero wavelet and scaling coefficients of an orthogonal wavelet [21], which can be characterized by its vanishing moment and support size [22].

A function with stronger high-frequency components can be better represented with a sparser set of coefficients derived from a wavelet with a larger number of vanishing moments, while a smaller support size leads to fewer high-amplitude coefficients [23]. For any orthogonal wavelet with p vanishing moments, a support size of at least $2p - 1$ is required [23]. For example, the Haar wavelet has the shortest support size among all orthogonal wavelets, and it has only one vanishing moment, which is insufficient to reconstruct time-varying sig-

nals without introducing artifacts. The Daubechies wavelets, generalized from the Haar wavelet, yield a minimum support size of $2p - 1$ for wavelets with p vanishing moments [23].

Wavelets like Symlets and Coiflets, derived from Daubechies wavelets, also have the potential for quantum sensing. Both Coiflet and Symlet wavelets have better symmetry than Daubechies wavelets [22], and the scaling function of the Coiflet is designed with vanishing moments, which is more suitable for reconstructing complex signals with higher smoothness [23], [24].

When applying the inverse discrete wavelet transform to reconstruct time-varying signals with only a small set of coefficients, some distortion may appear near the signal edge [25]. Such edge effect can be resolved by extending the total sensing time beyond the duration of the desired signal and then discarding the restored signals at both ends.

In this work, the generalized Daubechies wavelets are proposed to modulate the MW control sequences for quantum sensing. Multi-resolution analysis of an arbitrary magnetic signal is achieved by utilizing multiple qubit sensors, with each manipulated by an MW sequence mimicking a specific wavelet function, which is scaled and translated from the mother wavelet function. Each corresponding scaling or wavelet coefficient is determined from the readout of different qubits.

The rest of the work is organized as follows. The formulations and quantum sensing protocols are presented in Section II, the simulation results are discussed in Section III, and some conclusions are drawn in Section IV.

II. FORMULATIONS

Before conducting a generalized wavelet decomposition, the mother wavelet function $\psi(\tilde{t})$ and scaling function $\phi(\tilde{t})$ are dilated and translated to form orthonormal bases $\{\psi_m^n(\tilde{t})\}$ and $\{\phi_m^n(\tilde{t})\}$, respectively, where $\tilde{t} \in [0, T_w]$, and T_w is the wavelet support. For Daubechies wavelet with p vanishing moments (dbp), with $T_w = 2p - 1$ [23]. Both the mother wavelet $\psi(\tilde{t})$ and the scaling function $\phi(\tilde{t})$ are normalized such that their L_2 -norms are equal to one [26].

To measure a signal over $t \in [0, T_s]$, with a total sensing time of T_s , the linear time stretching relation

$$\tilde{t} = \frac{T_w}{T_s} t \quad (1)$$

is imposed to scale the n th wavelet and scaling functions of the m th scale as [23]

$$\begin{aligned} \psi_m^n(t) &= 2^{m/2} \psi \left(2^m \frac{T_w}{T_s} t - n \right) \\ \phi_m^n(t) &= 2^{m/2} \phi \left(2^m \frac{T_w}{T_s} t - n \right), \end{aligned} \quad (2)$$

with $m = J, J + 1, \dots, M$ and $n = 0, 1, \dots, N_m - 1$, where J is the minimum scale, M is the maximum scale, and N_m is the number of translated functions in the m th scale.

A time-varying signal $B_z(t)$ with finite energy can be represented in terms of the generalized wavelet basis as [23], [27]

$$B_z(t) \simeq \sum_{n=0}^{N_J-1} d_J^n \phi_J^n + \sum_{m=J}^M \sum_{n=0}^{N_m-1} c_m^n \psi_m^n(t), \quad t \in [0, T_s] \quad (3)$$

with the wavelet coefficient

$$c_m^n = \frac{T_w}{T_s} \int_0^{T_s} \psi_m^n(t) B_z(t) dt \quad (4)$$

and the scaling coefficient

$$d_J^n = \frac{T_w}{T_s} \int_0^{T_s} \phi_J^n(t) B_z(t) dt \quad (5)$$

A total of $N_J + \sum_{m=J}^M N_m$ qubits are required to implement (3),

with each qubit used to estimate one of c_m^n or d_J^n . It is assumed that each qubit is controlled with an independent MW control sequence, which is elaborated in Sec.II-B. These estimated coefficients are then used to reconstruct a time-varying field via an inverse wavelet transform.

The low-frequency approximation of the signal is first acquired by using the scaling coefficients of the J th scale. Then, high-frequency details are superposed to reconstruct a smooth signal. If larger J is chosen, the edge effect in low-frequency approximations can be better mitigated at the cost of requiring more scaling coefficients.

Next, we will define the system Hamiltonian and control Hamiltonian, establish the relation between wavelet functions and the MW control sequences, and formulate the time evolution of the qubit and its probability readout.

A. SYSTEM HAMILTONIAN

The time evolution of the quantum state in a qubit sensor can be simulated in terms of a Hamiltonian determined by the external signal and the MW control sequence. Without loss of generality, an external magnetic field $B_z(t)$ is assumed, which is characterized with a Hamiltonian in the lab frame as

$$H_s(t) = \frac{\hbar \omega_0 B_z(t)}{2} \sigma_z \quad (6)$$

where σ_z is the Pauli z matrix.

The MW control sequence is characterized with a control Hamiltonian in the lab frame as

$$H_c(t) = \hbar \Omega(t) \cos[\omega_c t + \phi(t)] \sigma_x \quad (7)$$

where σ_x is the Pauli x matrix, $\Omega(t)$ and $\phi(t)$ are the amplitude and phase, respectively, of the MW control field with carrier frequency ω_c .

Thus, the total Hamiltonian of a qubit in the lab frame is

$$H_d(t) = H_0 + H_s(t) + H_c(t) \quad (8)$$

with $H_0 = \hbar \omega_0 \sigma_z / 2$, where ω_0 is the Larmor frequency. By applying an unitary transformation operator

$$U_r = e^{-i \omega_0 t \sigma_z / 2} \quad (9)$$

the Hamiltonian in (8) can be transformed to the rotating frame, referring to H_0 , as

$$\begin{aligned} H_d^r(t) &\simeq U_r^\dagger H_d U_r - i\hbar U_r^\dagger \dot{U}_r \\ &= \frac{\hbar\gamma_e B_z(t)}{2} \sigma_z + \frac{\hbar\Omega(t)}{2} [\cos\phi(t)\sigma_x + \sin\phi(t)\sigma_y] \\ &\simeq \frac{\hbar\gamma_e B_z(t)}{2} \sigma_z + \frac{\hbar\Omega(t)}{2} \sigma_y \end{aligned} \quad (10)$$

where we set $\phi(t) = \pi/2$ in the last step.

B. RELATIVE PHASE ACCUMULATION

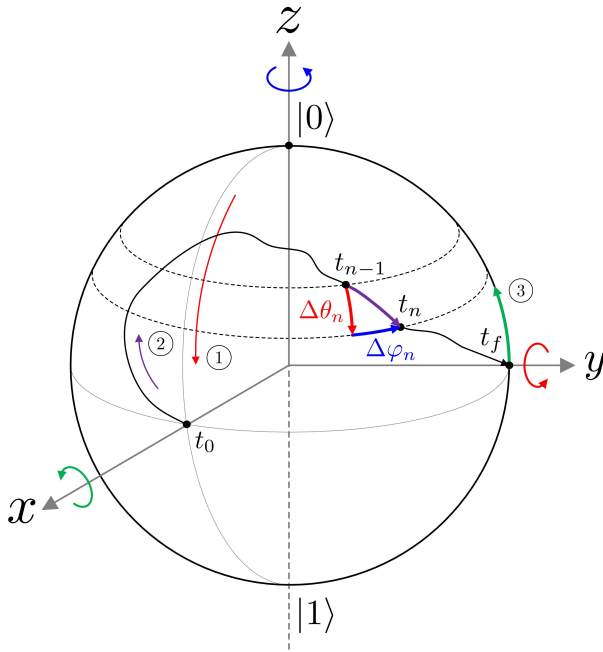


FIGURE 1. Time evolution of qubit state driven by an external magnetic signal $B_z(t)$ to spin about z axis (blue circle) and the microwave control sequence to spin about x axis (green circle) or y axis (red circle). By exerting a $(\pi/2)_y$ -pulse, the qubit state evolves from the north pole to the x axis along path ①. From $t = t_0$ to $t = t_f$, the qubit state evolves along path ② to the y axis under a σ_y -control Hamiltonian and a σ_z -signal Hamiltonian. At $t = t_f$, a $(\pi/2)_x$ -pulse is exerted to transform the qubit to the readout state along path ③. In an infinitesimal period $\Delta t_n = t_n - t_{n-1}$, the control Hamiltonian induces zenith angle change $\Delta\theta_n$ and the signal Hamiltonian induces azimuth angle change $\Delta\varphi_n$, causing an effective path marked in purple.

Fig.1 shows the time evolution of qubit state on the Bloch sphere to demonstrate how the quantum sensing protocol is implemented in three stages to reconstruct a time-varying magnetic field $B_z(t)$:

- ① Apply a $(\pi/2)_y$ -pulse
- ② Evolve the qubit state under the system Hamiltonian $H_d^r(t)$ in (10)
- ③ Apply a $(\pi/2)_x$ -pulse

By applying a $(\pi/2)_y$ -pulse to the initial state at the north pole, the qubit state jumps from $|0\rangle$ to $|\psi_1\rangle$ on the x axis at $t = t_0$, with

$$|\psi_1\rangle = |\psi_e(t_0)\rangle = R_y(\pi/2)|\psi_0\rangle = \frac{1}{\sqrt{2}}(|0\rangle + |1\rangle) \quad (11)$$

Then, the qubit state evolves under the Hamiltonian in (10) for a total sensing time of T_s , with the time evolution operator

$$\begin{aligned} U_e(t_0 + T_s, t_0) &= \exp \left\{ -\frac{i}{\hbar} \int_{t_0}^{t_0+T_s} H_d^r(t') dt' \right\} \\ &\simeq e^{-i(\varphi/2)\sigma_z} \end{aligned} \quad (12)$$

where φ is an effective accumulated phase.

As shown in Fig.1, during an infinitesimal period $\Delta t_n = t_n - t_{n-1}$, the control Hamiltonian embedding σ_y and the signal Hamiltonian embedding σ_z induce an infinitesimal change $\Delta\theta_n$ in the latitude and $\Delta\varphi_n$ in the longitude, respectively, of the qubit state on the Bloch sphere. The purple trace marks the effective state transition. The qubit state after imposing the operator in (12) becomes

$$\begin{aligned} |\psi_2\rangle &= |\psi_e(T_s)\rangle = U_e(T_s, 0)|\psi_e(0)\rangle \\ &= \frac{1}{\sqrt{2}}e^{-i\varphi/2}(|0\rangle + e^{i\varphi}|1\rangle) \end{aligned} \quad (13)$$

where we set $t_0 = 0$ without loss of generality.

The MW control sequence is designed such that the state $|\psi_2\rangle$ falls on the equatorial plane of the Bloch sphere. Finally, a $(\pi/2)_x$ -pulse is exerted to convert the qubit state $|\psi_2\rangle$ to a final state

$$|\psi_f\rangle = R_x(\pi/2)|\psi_2\rangle = \frac{1}{2}e^{-i\varphi/2} \begin{bmatrix} 1 - ie^{i\varphi} \\ -i + e^{i\varphi} \end{bmatrix} \quad (14)$$

The probability of the system staying at $|0\rangle$ is calculated as

$$P = |\langle 0|\psi_f\rangle|^2 = \frac{1}{2}(1 + \sin\varphi) \quad (15)$$

and the accumulated phase is

$$\varphi = \sin^{-1}(2P - 1) \quad (16)$$

Given a constant Hamiltonian $H_s = (\hbar\gamma_e b_z/2)\sigma_z$, the qubit state will rotate about the z axis of the Bloch sphere, and the effective phase accumulated over a period of Δt will be

$$\varphi = \int_0^{\Delta t} \alpha\gamma_e b_z dt \quad (17)$$

If the qubit state lies at a zenith angle θ , the effective modulation constant will be $\alpha = \pm \sin\theta$, where the sign changes whenever the qubit state passes either pole ($|0\rangle$ or $|1\rangle$) of the Bloch sphere under a control Hamiltonian which embeds σ_x or σ_y .

If the qubit state happens to be on the equatorial plane, the phase can be accumulated to the maximum extent, with $\alpha = \pm 1$. We can manipulate the modulation constant α in $[-1, 1]$ by applying a proper control Hamiltonian to change the latitude and the number of times the qubit state passes the poles.

C. WAVELET-MODULATED MW CONTROL SEQUENCE

By designing the amplitude $\Omega(t)$ of the MW control sequence in (10) with generalized wavelet functions, in the presence of a signal $B_z(t)$, the qubit state can be manipulated to accumulate relative phase by different rates at different latitudes during the sensing period, and the resulting readout probability is related to the wavelet coefficients.

Since the range of mother wavelet function ψ of generalized wavelets maybe wider than $[-1, 1]$. To implement the required modulation constants in terms of the wavelet functions, the latter are first normalized as

$$\bar{\psi}_m^n(t) = \frac{\psi_m^n(t)}{2^{m/2}A_0} \quad (18)$$

to ensure $|\bar{\psi}_m^n(t)| \leq 1$ for all t , where A_0 is a normalization constant.

Then, the planned zenith angle will be

$$\theta_m^n(t) = \sin^{-1} \bar{\psi}_m^n(t) \quad (19)$$

and the planned amplitude will be

$$\Omega_m^n(t) = \frac{\Delta\theta_m^n(t)}{\Delta t} \quad (20)$$

so that the qubit state can be evolved to the targeted latitude $\theta_m^n(t)$ and accumulate $\Delta\theta_m^n(t)$ during Δt .

Based on this idea, the quantum sensing protocol is designed as follows. Given the initial state $|0\rangle$, the qubit evolves under a time-varying MW control field (sequence) modulated by $\bar{\psi}_m^n(t)$ with amplitude $\Omega_m^n(t)$. The evolution operator is $U_e(t_{mi}^n, t_{mf}^n)$, where $[t_{mi}^n, t_{mf}^n]$ is the interval within which $\psi_m^n(t)$ has non-zero value, with $0 < t_{mi}^n < t_{mf}^n < T_s$, and the accumulated phase is

$$\varphi_m^n = \gamma_e \int_{t_{mi}^n}^{t_{mf}^n} \bar{\psi}_m^n(t) B_z(t) dt \quad (21)$$

Then, a $(\pi/2)_x$ -pulse is exerted to transform $|\psi_2\rangle$ state to an observable readout state $|\psi_f\rangle$, from which the probability of the qubit state remaining at $|0\rangle$ is calculated as

$$P_m^n = |\langle 0 | \psi_f \rangle|^2 = \frac{1}{2}(1 + \sin \varphi_m^n) \quad (22)$$

and the accumulated phase is determined as

$$\varphi_m^n = \sin^{-1}(2P_m^n - 1) \quad (23)$$

Finally, the wavelet coefficient defined in (4) can be related to the accumulated phase in (21) as

$$c_m^n = \frac{T_w}{T_s} \int_0^{T_s} \psi_m^n(t) B_z(t) dt = \frac{T_w}{T_s} \frac{2^{m/2} A_0}{\gamma_e} \varphi_m^n \quad (24)$$

The scaling coefficient d_m^n can be determined in a similar manner by modulating $\Omega_m^n(t)$ with the respective scaling function $\phi_m^n(t)$.

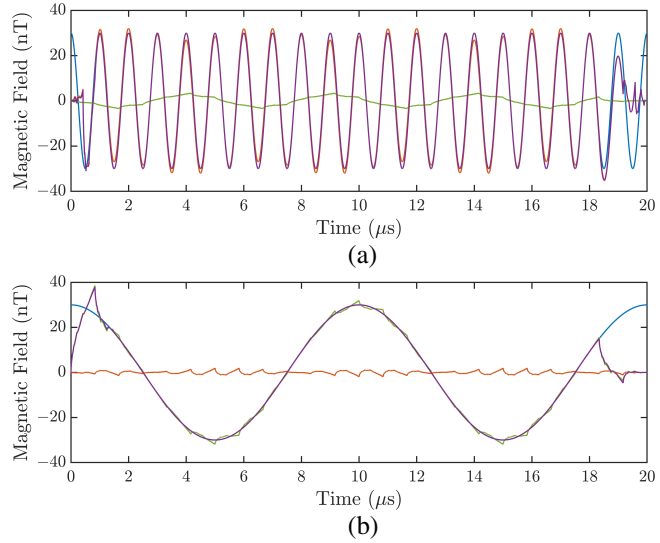


FIGURE 2. Quantum sensing of a single-tone magnetic field using MW control sequences based on db2 wavelet with $J = 3$ and $M = 8$. The signal frequency is (a) 1 MHz and (b) 100 kHz. —: True waveform, - - -: low-frequency approximation, - - : high-frequency details, - - - -: reconstructed waveform.

III. SIMULATIONS AND DISCUSSIONS

A. CONTRIBUTIONS OF SCALING AND WAVELET COEFFICIENTS

We first investigate how scaling and wavelet coefficients contribute to the reconstruction of different frequency components in a magnetic signal. The wavelet synthesis formula in (3) is split into

$$B_z^\ell(t) = \sum_{n=0}^{N_J-1} d_J^n \phi_J^n \quad (25)$$

$$B_z^h(t) = \sum_{m=J}^M \sum_{n=0}^{N_m-1} c_m^n \psi_m^n(t) \quad (26)$$

representing low-frequency approximation and high-frequency details, respectively. Figs.2(a) and 2(b) show the reconstruction of single-tone signals at 1 MHz and 100 kHz, respectively, where we choose the minimum scale of $J = 3$ and the maximum scale of $M = 8$.

Fig.2(a) shows the wavelet coefficients (orange) dominate the reconstruction of a high-frequency signal. On the other hand, Fig.2(b) shows the scaling coefficients dominate the reconstruction of the low-frequency signal. By deduction, an arbitrary waveform composed of various frequency components can be successfully reconstructed using the Daubechies wavelet-based quantum sensing protocol with both scaling and wavelet coefficients.

B. CHOICE OF MINIMUM SCALE

Next, we discuss how the choice of minimum scale J affects the reconstruction fidelity. Fig.3 shows the quantum sensing of a single-tone magnetic field at 500 kHz using MW control sequences based on db2 wavelet, with the number of scales fixed as $M - J = 5$.

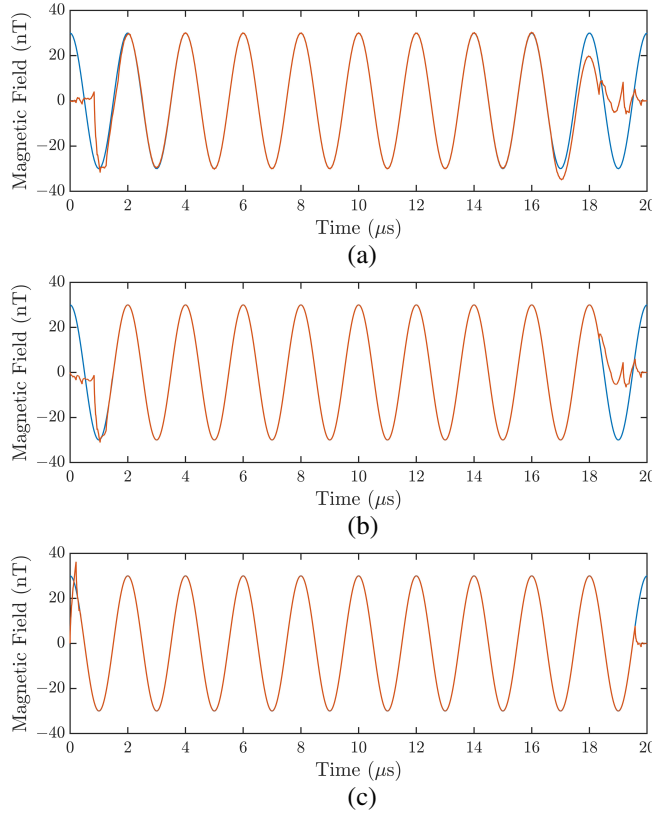


FIGURE 3. Quantum sensing of a single-tone magnetic field at 500 kHz using MW control sequences based on db2 wavelet, the number of scales is fixed as $M = J = 5$, (a) $J = 1$, (b) $J = 3$, and (c) $J = 5$. —: True waveform, - - -: reconstructed waveform.

Fig.3 shows that as J increases, the edge effect is squeezed near the beginning and end of the signal period. However, the number of required wavelet and scaling coefficients increases as J (and M) increases, implying that more quantum sensors are required. Hence, there is a trade-off between the reduction of edge effect and the required resources. Moreover, Fig.3(c) shows that when $J = 5$ is chosen, the edge effect only affects less than 10% of the interval within the total sensing time. Thus, in the following simulations, we choose the minimum scale of $J = 5$ and only consider the reconstructed waveform in the central segment ($2 \leq t \leq 18\mu\text{s}$) without the edge effect.

C. DAUBECHIES WAVELETS OF DIFFERENT VANISHING MOMENTS

The Haar wavelet, or the db1 wavelet, is a well-known wavelet with a square shape. The Haar wavelet resembles the spin-echo (SE) MW sequence for qubit control in quantum sensing applications. A SE sequence consists of a $(\pi/2)$ -pulse, a π -pulse, and another $(\pi/2)$ -pulse, with an equal time interval inserted between two subsequent pulses. The extracted Haar coefficients can reconstruct the signal shape but with some step-like artifacts attributed to the square shape of the Haar wavelets.

Fig.4(a) shows a Haar wavelet-reconstructed single-tone magnetic field, $B_{1z}(t) = 30 \cos(2\pi f_1 t)$ (nT), with $f_1 = 1$

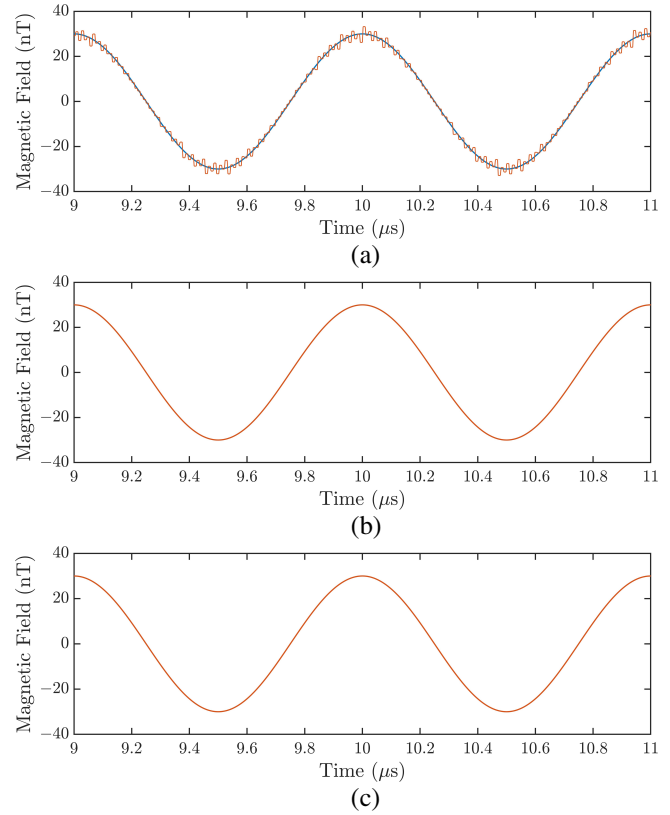


FIGURE 4. Central segment of reconstructed single-tone magnetic field $B_{1z}(t)$, free from edge effect, using MW control sequences based on different wavelets, with $J = 5$ and $M = 10$. (a) Haar (Daubechies-1) wavelet, (b) Daubechies-2 wavelet, (c) Daubechies-4 wavelet. —: True waveform, - - -: reconstructed waveform.

TABLE 1. NRMSE of quantum sensing based on Daubechies- p wavelet, $J = 5$, $M = 10$.

wavelet	NRMSE value
Daubechies-1 (Haar)	5.506×10^{-3}
Daubechies-2	3.481×10^{-9}
Daubechies-3	1.573×10^{-9}
Daubechies-4	6.464×10^{-10}
Daubechies-5	2.070×10^{-10}

MHz and a total sensing time of $T_s = 20\mu\text{s}$. Obvious step-like artifacts are induced, which are attributed to the square shape of the Haar wavelets. This problem can be effectively mitigated by using Daubechies wavelets with a higher number of vanishing moments.

The dbp wavelets are smoother as p increases. Designing a continuous-wave (CW) MW sequence to mimic dbp wavelets is expected to reduce the distortion in the reconstructed waveform.

Figs.4(b) and 4(c) show that the reconstructed waveform using db2 and db4 becomes smoother. However, as the number of vanishing moments p increases, the time interval affected by edge effects increases at both edges because the energy in the wavelet function is more concentrated in its middle segment. Since this edge effect is inevitable, we will focus on the reconstructed waveforms in the central segment

($2 \leq t \leq 18\mu\text{s}$), ignoring the small segment at both edges.

To quantify the error between the reconstructed waveform $\tilde{B}_z(t)$ and the true waveform $B_z(t)$, a normalized root mean square error (NRMSE) between these two waveforms is defined as

$$\text{NRMSE}(\tilde{B}_z, B_z) = \frac{\left[\int_{\epsilon}^{T_s - \epsilon} |\tilde{B}_z(t) - B_z(t)|^2 dt \right]^{1/2}}{\left[\int_{\epsilon}^{T_s - \epsilon} |B_z(t)|^2 dt \right]^{1/2}} \quad (27)$$

where ϵ is the interval at both ends that manifest. Table 1 lists the NRMSE with Daubechies wavelets of different vanishing moments.

Figs.4(b) and 4(c) show that the central segment of the waveform is accurately estimated when $p \geq 2$. The NRMSE values listed in Table 1 indicate that the reconstruction fidelity using db2 wavelets is significantly improved over that using Haar wavelets.

It is worth mentioning that both the required wavelet and scaling coefficients increase as the scale m increases. Table 1 reveals that when switching from the Haar wavelet to the db2 wavelet, the NRMSE drops by six orders. However, when applying Daubechies wavelet with $p \geq 2$, the improvement is limited. Hence, the db2 wavelet is adopted in the subsequent simulations, unless specified otherwise.

D. DAUBECHIES-2 (DB2) WAVELET WITH DIFFERENT MAXIMUM SCALES

Next, we fix the minimum scale to $J = 5$ and vary the maximum scale of the db2 wavelet to study the effects of detail levels on waveform reconstruction. Fig.5 shows the reconstruction waveforms with $M = 5$ and $M = 14$, respectively. As M increases, the fidelity of waveform reconstruction is significantly improved, as manifested in Table 2 that the NRMSE decreases with larger M or more high-frequency details. The NRMSE saturates as M is larger than 12, implying that most of the high-frequency components are included using wavelet coefficients of scale $m \leq 12$.

TABLE 2. NRMSE of quantum sensing based on Daubechies-2 Wavelet with $J = 5$ and different maximum scales.

scale	NRMSE value	scale	NRMSE value
5	1.609×10^{-2}	10	1.654×10^{-8}
6	1.062×10^{-3}	12	2.628×10^{-9}
8	4.212×10^{-6}	14	2.617×10^{-9}

E. RECONSTRUCTION OF VARIOUS WAVEFORMS

Next, we will validate if the proposed method can be applied to reconstruct different waveforms other than single-tone signals. Figs.6(a) and 6(b) show the reconstruction of a triple-tone magnetic field, including $B_{1z}(t)$, with a large DC offset as

$$B_{2z}(t) = B_{1z}(t) + 20 \cos(2\pi f_2 t) + 40 \sin(2\pi f_3 t) + 80 \text{ (nT)} \quad (28)$$

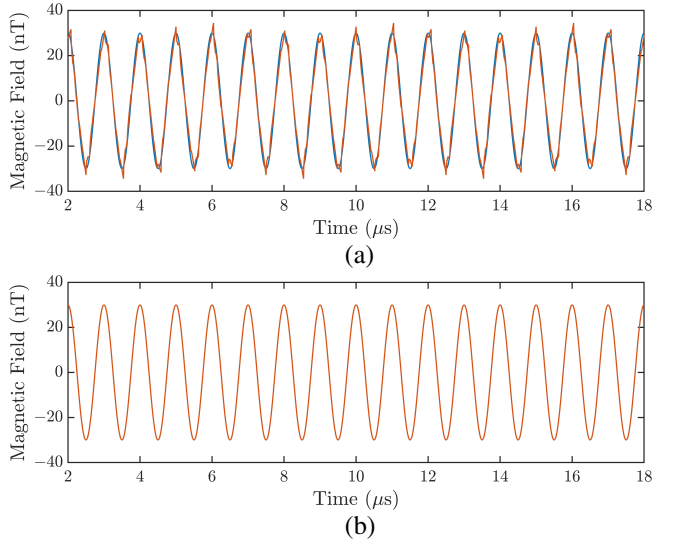


FIGURE 5. Quantum sensing of a single-tone magnetic field $B_{1z}(t)$ using MW control sequences based on Daubechies-2 wavelet, $J = 5$, (a) $M = 5$, (b) $M = 14$. —: True waveform, - - -: reconstructed waveform.

where $f_2 = 0.3$ MHz and $f_3 = 2.3$ MHz. The NRMSE of the reconstructed waveform in Fig.6(b) is 2.344×10^{-7} , larger than that of the single-tone field, indicating that the high-frequency components in $B_{2z}(t)$ are not entirely captured with $M = 10$.

Fig.6(c) shows a decently reconstructed spin-bath noise field $B_{3z}(t)$, which follows the Lorentzian distribution

$$S(\omega) = \frac{\Delta^2 \tau_c}{\pi} \frac{1}{1 + (\omega \tau_c)^2} \quad (29)$$

to mimic the spin-bath noise in quantum sensors based on nitrogen-vacancy (NV) centers, where Δ is the coupling strength and τ_c is the correlation time [28].

Fig.7(a) shows the magnified version of some segments, away from both ends, in Fig.6(c). Only minor reconstruction artifacts appear over these segments. The NRMSE is 1.7812×10^{-4} , three-order larger than the two waveforms shown in Fig.6, owing to obvious edge effect near the ends of the sensing interval.

To mitigate this problem, the maximum scale is increased to $M = 14$, including more high-frequency components. Fig.7(b) shows the reconstructed waveforms, with the NRMSE reduced to 6.682×10^{-8} .

Next, the same method is applied to reconstruct noise waveform $B_{3z}(t)$. The NRMSE values listed in Table 3 manifest that the noise waveform can be reconstructed at higher accuracy with an increasing number of vanishing moments.

Table 4 lists the NRMSE values based on db2 wavelet with $J = 5$ and different maximum scales. The NRMSE value with $M = 5$ or $M = 6$ for noise waveform with high-frequency components is significantly large because only low-level details are considered. The NRMSE value drops as the maximum scale increases, suggesting that more high-frequency details are needed to reconstruct noise waveform.

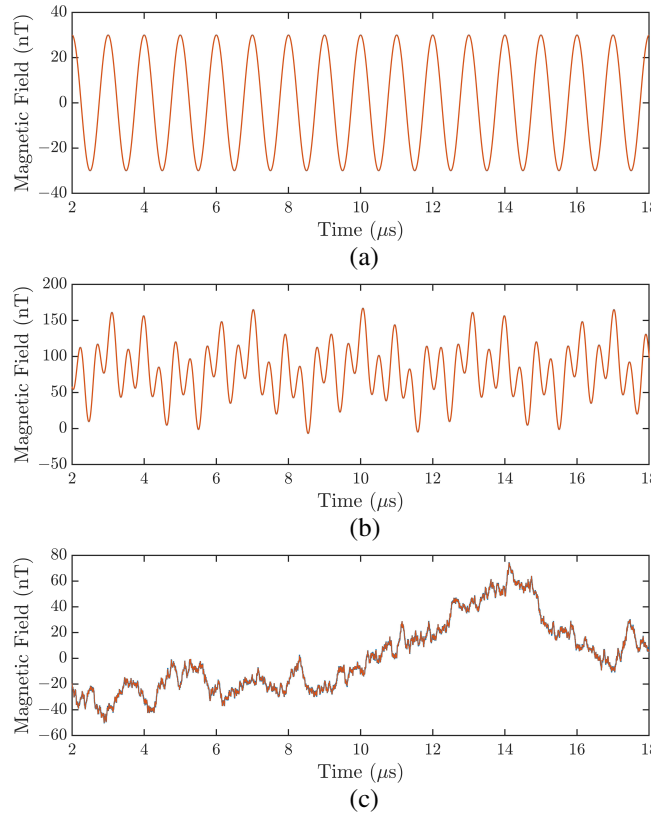


FIGURE 6. Quantum sensing of magnetic waveforms using MW control sequences based on db2 wavelet, with $J = 5$ and $M = 10$, (a) single-tone waveform $B_{1z}(t)$, (b) triple-tone waveform with large DC offset $B_{2z}(t)$, and (c) Lorentzian noise waveform $B_{3z}(t)$, with $\Delta = 30$ kHz, $\tau_c = 10\mu\text{s}$. ---: true waveform, —: reconstructed waveform.

TABLE 3. NRMSE of quantum sensing on noise waveform $B_{3z}(t)$ based on Daubechies- p wavelet with $J = 5$ and $M = 10$.

wavelet	NRMSE value
Daubechies-1 (Haar)	6.034×10^{-3}
Daubechies-2	1.419×10^{-4}
Daubechies-3	5.361×10^{-5}
Daubechies-4	2.633×10^{-5}
Daubechies-5	1.539×10^{-5}

Notice that the spin-bath noise $B_{3z}(t)$ has a broadband spectrum, the NRMSE values of its reconstruction listed in Tables 3 and 4 are significantly larger than their counterparts of single-tone signal reconstruction.

The results shown in Fig.6 and Fig.7 validate the efficacy of the proposed approach of applying the Daubechies wavelets to modulate qubit control for reconstructing an arbitrary waveform composed of multiple tones and a dc offset.

In practice, physical quantum sensors based on an ensemble of NV centers are immersed in spin-bath noise, which tends to deteriorate the sensor sensitivity in measuring a weak magnetic field. Fig.7(b) manifests that the proposed protocol is capable of capturing noisy signals with decent fidelity, confirming that the Daubechies scaling and wavelet coefficients extracted from qubits with the proposed approach can effectively restore noisy spectral information. The infor-

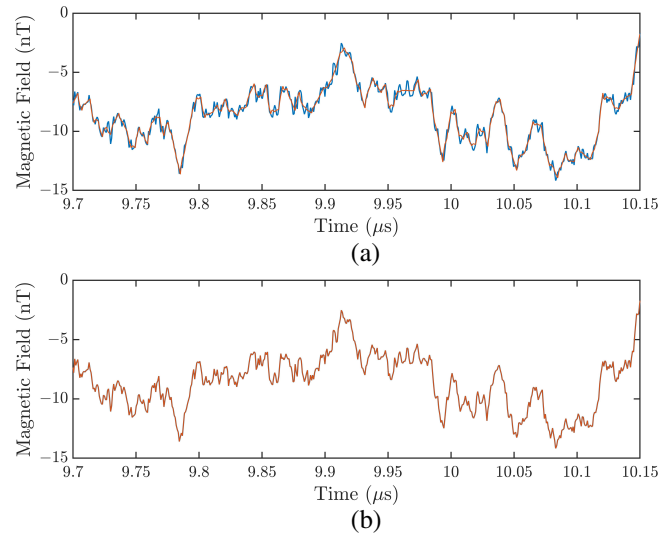


FIGURE 7. Magnified noisy signal quantum sensed with MW control sequences based on db2 wavelet, $J = 5$, (a) $M = 10$, (b) $M = 14$. ---: True waveform, —: reconstructed waveform.

TABLE 4. NRMSE of quantum sensing on noise waveform $B_{3z}(t)$ based on Daubechies-2 wavelet with $J = 5$ and different maximum scales.

scale	NRMSE value	scale	NRMSE value
5	1.539	10	1.419×10^{-4}
6	2.065×10^{-1}	12	3.217×10^{-6}
8	1.781×10^{-3}	14	6.682×10^{-8}

mation extracted from all the qubits in the NV ensemble can be averaged to reconstruct the true waveform faithfully.

The proposed sensing protocol can also be extended to study other practical factors that could deteriorate the sensitivity of physical quantum sensors.

IV. CONCLUSIONS

A Daubechies wavelet-based quantum sensing protocol is proposed for the first time to reconstruct an arbitrary magnetic waveform with high fidelity. Mathematical formulation inspired by intuitive operation on the Bloch sphere is derived to bring out the generalized discrete wavelet transform for quantum sensing of arbitrary waveforms. The efficacy and accuracy of the proposed method are validated by simulations. Different parameters of wavelets on the reconstructed waveform are analyzed. Edge effects are observed near both ends of the sensing interval, which can be solved by extending the total sensing time and then discarding the reconstructed waveform at both edges. The wavelet scales and vanishing moments can be varied contingent upon the waveform or spectrum to be measured. The proposed method can be extended to various quantum sensing applications, including the evaluation of quantum sensors for reconstructing fast time-varying magnetic fields before physical implementations.

REFERENCES

- [1] K. Bian *et al.*, “Nanoscale electric-field imaging based on a quantum sensor and its charge-state control under ambient condition,” *Nat. Commun.*, vol. 12, no. 1, Apr. 2021.

- [2] C. T. Fancher, D. R. Scherer, M. C. St. John, and B. L. S. Marlow, "Rydberg atom electric field sensors for communications and sensing," *IEEE Trans. Quantum Eng.*, vol. 2, 3501313, Mar. 2021.
- [3] J. M. Schloss, J. F. Barry, M. J. Turner, and R. L. Walsworth, "Simultaneous broadband vector magnetometry using solid-state spins," *Phys. Rev. Appl.*, vol. 10, no. 3, 034044, Sep. 2018.
- [4] M. I. Ibrahim, C. Foy, D. Englund, and R. Han, "High-scalability CMOS quantum magnetometer with spin-state excitation and detection of diamond color centers," *IEEE J. Solid-state Circuits*, vol. 56, pp. 1001-1014, Mar. 2021.
- [5] J. Fan *et al.*, "Germanium-vacancy color center in diamond as a temperature sensor," *ACS Photonics*, vol. 5, pp. 765-770, Jan. 2018.
- [6] M. W. Doherty *et al.*, "Electronic properties and metrology applications of the diamond NV⁻ center under pressure," *Phys. Rev. Lett.*, vol. 112, no. 4, 047601, Jan. 2014.
- [7] X. Lyu *et al.*, "Strain quantum sensing with spin defects in hexagonal boron nitride," *Nano Letters*, vol. 22, no. 16, pp. 6553-6559, Aug. 2022.
- [8] F. Poggiali, P. Cappellaro, and N. Fabbri, "Optimal control for one-qubit quantum sensing," *Phys. Rev. X*, vol. 8, Jun. 2018.
- [9] V. Frey *et al.*, "Application of optimal band-limited control protocols to quantum noise sensing," *Nat. Commun.*, vol. 8, Dec. 2017.
- [10] J. Zopes and C. L. Degen, "Reconstruction-free quantum sensing of arbitrary waveforms," *Phys. Rev. Appl.*, vol. 12, Nov. 2019.
- [11] N. Xu *et al.*, "Wavelet-based fast time-resolved magnetic sensing with electronic spins in diamond," *Phys. Rev. B*, vol. 93, Apr. 2016.
- [12] E. Magesan, A. Cooper, H. Yum, and P. Cappellaro, "Reconstructing the profile of time-varying magnetic fields with quantum sensors," *Phys. Rev. A*, vol. 88, Sep. 2013.
- [13] B. Kantsepolsky, I. Aviv, R. Weitzfeld, and E. Bordo, "Exploring quantum sensing potential for systems applications," *IEEE Access*, vol. 11, pp. 31569-31582, Mar. 2023.
- [14] C.-W. Kiang and J.-F. Kiang, "Quantum sensing of geomagnetic fluctuations and noise spectroscopy with hybrid short Ramsey-Haar wavelet method and NV ensembles," *in revision*.
- [15] J. M. Barry *et al.*, "Optical magnetic detection of single-neuron action potentials using quantum defects in diamond," *Proc. Nat. Academy Sci.*, vol. 113, no. 49, pp. 14133-14138, Dec. 2016.
- [16] K. L. Jensen *et al.*, "Non-invasive detection of animal nerve impulses with an atomic magnetometer operating near quantum limited sensitivity," *Sci. Rep.*, vol. 6, no. 1, Jul. 2016.
- [17] H. Morishita *et al.*, "Spin-dependent dynamics of photocarrier generation in electrically detected nitrogen-vacancy-based quantum sensing," *Phys. Rev. Appl.*, vol. 19, no. 3, Mar. 2023.
- [18] M. Baumgartner *et al.*, "Spatially and time-resolved magnetization dynamics driven by spin-orbit torques," *Nat. Nanotechnol.*, vol. 12, no. 10, pp. 980-986, Aug. 2017.
- [19] T. J. Green, J. Sastrawan, H. Uys, and M. J. Biercuk, "Arbitrary quantum control of qubits in the presence of universal noise," *New J. Phys.*, vol. 15, no. 9, 095004, Sep. 2013.
- [20] G. P. Nason, "Choice of wavelet smoothness, primary resolution and threshold in wavelet shrinkage," *Statistics and Computing*, vol. 12, pp. 219-227, Jul. 2002.
- [21] C. Vonesch, T. Blu, and M. Unser, "Generalized Daubechies wavelet families," *IEEE Trans. Signal Process.*, vol. 55, no. 9, pp. 4415-4429, Sep. 2007.
- [22] T. Guo, T. Zhang, E. Lim, M. López-Benítez, F. Ma, and L. Yu, "A review of wavelet analysis and its applications: Challenges and opportunities," *IEEE Access*, vol. 10, pp. 58869-58903, 2022.
- [23] S. Mallat, *A Wavelet Tour of Signal Processing: The Sparse Way*, 3rd ed., Academic Press, 2009.
- [24] C. S. Burrus and I. E. Odegard, "Coiflet systems and zero moments," *IEEE Trans. Signal Process.*, vol. 46, no. 3, pp. 761-766, Mar. 1998.
- [25] D. Gogolewski, "Influence of the edge effect on the wavelet analysis process," *Measurement*, vol. 152, 107314, Feb. 2020.
- [26] S. Sinha, P. S. Routh, P. D. Anno, and J. P. Castagna, "Spectral decomposition of seismic data with continuous-wavelet transform," *Geophysics*, vol. 70, no. 6, pp. P19-P25, Nov. 2005.
- [27] S.-Y. Huang and Z. Bai, "Wavelets, advanced," in *Encyclopedia of Physical Science and Technology*, 3rd ed., R. A. Meyers, ed., Academic Press, 2003, pp. 753-771.
- [28] N. Bar-Gill *et al.*, "Suppression of spin-bath dynamics for improved coherence of multi-spin-qubit systems," *Nat. Commun.*, vol. 3, Jan. 2012.



CHOU-WEI KIANG received his B.S. degree in electrical engineering from National Taiwan University, Taipei, Taiwan, in 2022. He is currently a research assistant in the Quantum Electronics Laboratory, National Taiwan University. From 2020 to 2023, he was a research assistant in the Group of Electromagnetic Applications, National Taiwan University, where he worked on quantum sensing and remote sensing. His research interests include quantum science and engineering, quantum information processing, optics and electromagnetics, remote sensing, radar and sonar imaging, and signal processing applications.



JIAN-JIUN DING was born in 1973 in Taiwan. He received the Ph.D. degree in 2001 from National Taiwan University (NTU), Taipei, Taiwan. In 2006, he became an assistant professor in the Department of EE and the Graduate Institute of Communication Engineering (GICE), NTU. In 2012, he was promoted to an associate professor. In 2017, he was promoted to a professor. His current research areas include time-frequency analysis, linear canonical transforms, wavelet transforms, image processing, image compression, integer transforms, pattern recognition, face recognition, machine learning, etc.



JEAN-FU KIANG (Life Senior, IEEE) received his Ph.D. degree in electrical engineering from the Massachusetts Institute of Technology, Cambridge, MA, USA, in 1989. Since 1999, he has been a Professor with the Department of Electrical Engineering and Graduate Institute of Communication Engineering, National Taiwan University. His research interest is to explore different ideas, theories and methods on various electromagnetic phenomena and possible applications, including remote sensing, radar signal processing, antennas, phased arrays, propagation, scattering, communications, and so on. Some of his works can be viewed in his website: http://cc.ee.ntu.edu.tw/~jfkiang/selected_publications.html